Published by
NIGERIAN SOCIETY OF PHYSICAL SCIENCES
Available online @ https://asr.nsps.org.ng/index.php/asr

African Scientific Reports 5 (2026) 474

African Scientific Reports

Impact of level density models on the calculation of some theranostic radionuclides using EMPIRE code

Matthew Inalegwu Amanyi[a,b,*], Umaru Ibrahim[b], Kolo Matthew[c]

[a]*Department of Physics, Federal University of Health Sciences, Otukpo, Benue State, Nigeria*
[b]*Department of Physics, Nasarawa State University, Keffi, Nigeria*
[c]*Department of Physics, Federal University of Technology, Minna, Nigeria*

Abstract

Radioisotopes such as ^{67}Cu, ^{131}I, and ^{99m}Tc are used in nuclear medicine for diagnostic and therapeutic (theranostic) applications. Cross-section data for the nuclear reactions that produce these radioisotopes are essential for efficient production; however, experimental cross-section data remain limited for these isotopes. The reaction cross sections of the radioisotopes ^{67}Cu, ^{131}I, and ^{99m}Tc were evaluated using the nuclear reaction model code EMPIRE 3.2.3. The influence of nuclear level density (NLD) models on energy-dependent cross-section calculations was investigated for the reactions ^{68}Zn(p,2p)^{67}Cu, ^{70}Zn(p,α)^{67}Cu, ^{130}Te(d,n)^{131}I, ^{100}Mo(p,2n)^{99m}Tc, and ^{100}Mo(n,2n)^{99}Mo within an energy range from threshold to 70 MeV. Calculated energy-dependent cross-section functions were benchmarked against experimental data from the EXFOR database and evaluated nuclear data from International Atomic Energy Agency (IAEA) libraries. The results show clear sensitivity of the predicted cross sections to the selected NLD model. The cross-sections predicted by the nuclear level density models that showed the best agreement with the experimental data were 32 MeV (6.80 mb) for ^{68}Zn(p,2p)^{67}Cu, 17 MeV (17.79 mb) for ^{70}Zn(p,α)^{67}Cu, 12 MeV (99.94 mb) for ^{130}Te(d,n)^{131}I, and 18 MeV for both ^{100}Mo(p,2n)^{99m}Tc (994.78 mb) and ^{100}Mo(n,2n)^{99}Mo (1500 mb). Radionuclidic purity indices ranged from 1.93% to 17.27%, depending on the reaction channel. These results demonstrate the reliability of EMPIRE 3.2.3 for predicting cross sections and provide useful nuclear data for radionuclide production.

DOI: 10.46481/asr.2026.5.2.474

Keywords: EMPIRE 3.2.3, Medical radioisotopes, Level density models, Nuclear reaction cross sections

Article History:
Received: 10 March 2026
Received in revised form: 10 June 2026
Accepted for publication: 12 June 2026
Available online: 19 August 2026

© 2026 The Author(s). Published by the Nigerian Society of Physical Sciences under the terms of the Creative Commons Attribution 4.0 International license. Further distribution of this work must maintain attribution to the author(s) and the published article's title, journal citation, and DOI.

1. Introduction

Nuclear medicine is a specialized field that uses radioactive isotopes to diagnose and treat diseases through radiopharmaceuticals [1, 2]. Medically important radionuclides, including ^{67}Cu, ^{131}I, and ^{99m}Tc, are extensively used in diagnostic imaging and targeted radionuclide therapy because of their favorable decay characteristics and biological compatibility [2, 3]. Nevertheless, acquiring precise nuclear reaction cross-section data presents a considerable challenge, as experimental results from different laboratories frequently show incompleteness, inconsistency, and discrepancies across broad energy ranges [4, 5].

*Corresponding Author Tel. No.: +234-805-965-3485.
Email address: matthew.amanyi@fuhso.edu.ng (Matthew Inalegwu Amanyi)

Among the available nuclear reaction codes, the EMPIRE 3.2.3 system is particularly suitable because it integrates multiple nuclear reaction mechanisms within a unified computational framework [6]. The code incorporates internationally recommended nuclear input parameters from the Reference Input Parameter Library (RIPL-3), thereby improving the reliability of theoretical predictions across broad incident-energy ranges [6].

The calculated cross sections were benchmarked against experimental data retrieved from the EXFOR database and evaluated nuclear data libraries, including ENDF/B-VIII.0, IAEA Medical, IAEA-Therapeutic, and TENDL-2023 [4, 6, 7].

2. Materials and methods

2.1. Materials

The key materials used in this study were as follows.

1. EMPIRE code: The EMPIRE code was used to evaluate nuclear reaction cross sections. The code uses nuclear structure and reaction input parameters obtained from RIPL-3, including optical model potentials, level density parameters, and gamma-ray strength functions. These parameters were used without modification, except for the systematic variation of NLD models to investigate their impact on the calculated excitation functions.
2. EXFOR database: The EXFOR database was used to access experimental cross-section information for copper-67, iodine-131, and technetium-99m. It served as the primary source of experimental cross-section data for benchmarking the calculated excitation functions from EMPIRE 3.2.3. The retrieved datasets were selected based on data completeness, reported uncertainties, and consistency across different measurements.
3. ZVView plotting package: ZVView was used to generate excitation-function plots for each reaction channel, facilitating direct visual comparison between calculated and experimental cross sections. This allowed qualitative assessment of model performance, including agreement in peak cross-section values, peak energies, and overall excitation-function shapes.
4. Reference Input Parameter Library (RIPL-3): The nuclear model input parameters required for EMPIRE calculations were obtained from RIPL-3. RIPL-3 provides standardized and recommended nuclear reaction parameters, including optical model potentials, level density parameters, and gamma-ray strength functions.
5. Personal computer: A personal computer was used to perform computation-intensive simulations, including EMPIRE code calculations, and to store data and simulation outputs.
6. FORTRAN 77 compiler: A FORTRAN 77 compiler was used to execute the EMPIRE 3.2.3 code and any modifications made to it.
7. International Atomic Energy Agency (IAEA) resources: IAEA Nuclear Data Services (NDS) resources were used to access reference and evaluated nuclear data, including IAEA-Therapeutic, IAEA-Medical, and TENDL data.
8. Microsoft Excel: Microsoft Excel was used to store experimental and simulated data for statistical analysis.

2.2. Method

2.2.1. Compilation and validation of the experimental data

Experimental nuclear reaction cross-section data for the investigated reactions were obtained from the EXFOR database maintained by the International Atomic Energy Agency (IAEA) Nuclear Data Services. The database provides a comprehensive collection of experimentally measured nuclear reaction data, including reaction channels, target isotopes, projectile types, incident particle energies, measured cross sections, and associated uncertainties.

The retrieved datasets were screened to ensure their relevance to the production reactions and energy ranges considered in this study. Only datasets corresponding to the selected reaction channels and containing adequate experimental information were retained for further analysis. Where multiple datasets were available for a particular reaction, comparisons were performed to evaluate the consistency of the reported excitation functions in terms of peak cross sections, peak energies, and overall excitation-function trends.

In cases where discrepancies existed among different experimental measurements, the general behavior and trend of the available datasets were considered rather than relying solely on a single measurement. This approach minimized the influence of isolated deviations and provided a more representative basis for comparison with theoretical calculations.

The validated experimental datasets were subsequently used as benchmark data for assessing the performance of the EMPIRE 3.2.3 nuclear reaction code. Comparisons between calculated and experimental excitation functions were carried out using the reported cross-section values and uncertainties available in the EXFOR database. No additional normalization, correction, or re-evaluation of the experimental data was performed before the comparison. This procedure ensured that the assessment of the theoretical calculations was based on independently measured experimental data and enhanced the reliability of the validation process.

2.2.2. Nuclear level density models

Nuclear level density (NLD) is defined as the number of available nuclear energy levels per unit excitation energy at a given excitation energy. It is a fundamental quantity in statistical nuclear reaction theory, as it determines the probability of compound nucleus formation and decay. Within the Hauser–Feshbach formalism, the reaction cross section depends strongly on the density of accessible final states; hence, an accurate description of NLD is essential for reliable cross-section calculations [8, 9].

In this study, the impact of different NLD models on calculated excitation functions was investigated using the EMPIRE code. Four level density models available in EMPIRE were considered: the Enhanced Generalized Superfluid Model (EGSM), Generalized Superfluid Model (GSM), Gilbert–Cameron Model (GCM), and microscopic Hartree–Fock–Bogoliubov (HFB) model.

Gilbert–Cameron model (GCM). The Gilbert–Cameron model is a phenomenological composite model that combines a constant-temperature formulation at low excitation energies with a Fermi gas model at higher energies [10]. This allows it to account for discrete nuclear levels at low energies and statistical behavior at higher excitation energies. Because of its simplicity and reasonable accuracy, it is widely used in nuclear reaction calculations.

Generalized superfluid model (GSM). The Generalized Superfluid Model incorporates pairing correlations between nucleons and describes the transition of the nucleus from a superfluid state at low excitation energies to a normal Fermi gas state at higher energies [11]. This model introduces an energy-dependent level density parameter and provides improved predictions near reaction threshold energies where pairing effects are significant.

Enhanced generalized superfluid model (EGSM). The Enhanced Generalized Superfluid Model extends the GSM by including collective enhancement effects and improved treatment of shell corrections [11]. These additional features allow better representation of nuclear deformation and collective motion, which can significantly influence level density at intermediate excitation energies.

Hartree–Fock–Bogoliubov model (HFB). The Hartree–Fock–Bogoliubov model is a microscopic approach based on self-consistent mean-field theory, incorporating nucleon–nucleon interactions, shell effects, deformation, and pairing correlations explicitly [12]. Unlike phenomenological models, HFB does not rely on empirical parameter fitting, making it more fundamental, although its predictive accuracy depends on the underlying nuclear structure inputs.

2.2.3. Cross-section evaluation with EMPIRE 3.2.3

The medically relevant nuclear reactions investigated in this study were ^{68}Zn(p,2p)^{67}Cu, ^{70}Zn(p,α)^{67}Cu, ^{130}Te(d,n)^{131}I, ^{100}Mo(p,2n)^{99m}Tc, and ^{100}Mo(n,2n)^{99}Mo. For each reaction channel, the corresponding target nucleus, projectile type, incident energy range, and emitted particles were defined in the EMPIRE input file. The incident energy range was selected from the reaction threshold up to 70 MeV based on available experimental data and medical production relevance.

The EMPIRE 3.2.3 code was configured to use the Hauser–Feshbach statistical model for compound nucleus calculations together with pre-equilibrium reaction mechanisms. This enabled the calculation of both equilibrium and non-equilibrium contributions to the reaction cross sections.

Optical model parameters for neutrons, protons, deuterons, and alpha particles were obtained from RIPL-3. These parameters were used by EMPIRE to calculate transmission coefficients and particle interaction probabilities required for reaction modeling.

Four different NLD models available in EMPIRE 3.2.3 were investigated: EGSM, GSM, GCM, and the HFB microscopic model. Each model was applied separately for all reaction channels to evaluate its influence on the predicted excitation functions.

The prepared input files were executed using the FORTRAN-based EMPIRE 3.2.3 code on a high-performance computer system. The code generated theoretical excitation functions and reaction cross-section outputs for each reaction and level density model combination.

The calculated cross-section outputs generated by EMPIRE were extracted and organized into Microsoft Excel spreadsheets for further analysis. Peak cross sections, peak energies, and excitation-function trends were identified for each reaction channel.

The theoretical cross sections obtained from EMPIRE were compared with experimental data compiled from the EXFOR database and evaluated nuclear data libraries, such as ENDF/B-VIII.0, IAEA Medical, IAEA-Therapeutic, and TENDL-2023. This comparison was performed to determine the predictive performance of each level density model.

Finally, ZVView plotting software was used to plot the calculated excitation functions together with the experimental datasets. The agreement between theoretical and experimental results was evaluated based on peak position, peak magnitude, and overall excitation-function shape.

2.2.4. Method of analysis and visualization

The EMPIRE 3.2.3 results were statistically compared with available experimental nuclear reaction cross-section data. An important measure for this comparison was the percentage deviation, which measures the extent of agreement between theoretical and experimental values. The percentage deviation is given as

$$\%\Delta\sigma = \frac{\Sigma\left|\sigma_{\text{exp}} - \sigma_{\text{theo}}\right| + \sigma_{\text{error}}}{\sigma_{\text{error}}} \times 100\%, \tag{1}$$

where σ_{theo} is the theoretical cross section from EMPIRE 3.2.3, σ_{exp} is the experimental cross section, and σ_{error} is the experimental cross-section error.

The comparison between the calculated cross sections obtained from EMPIRE and the experimental cross sections retrieved from the EXFOR database was carried out by matching both datasets at corresponding incident particle energies. For each reaction channel, the theoretical excitation functions generated by EMPIRE were interpolated to the same energy points reported in the experimental measurements. At every corresponding energy value, the calculated cross section σ_{theo} was paired with the experimental cross section σ_{exp} and the associated experimental uncertainty $\Delta\sigma_{exp}$.

The absolute difference between the theoretical and experimental values was then determined for all matched energy points and normalized using the reported experimental uncertainty. The percentage deviation was subsequently computed using Eq. (1). This procedure enabled a quantitative evaluation of the agreement between the EMPIRE predictions and the experimentally measured nuclear reaction cross sections across the investigated energy range.

This approach gives a numerical estimate of the predictive strength of the nuclear reaction models and input parameters used in EMPIRE 3.2.3 [13].

3. Results and discussion

The calculated excitation functions obtained using the EMPIRE level density models (EGSM, GSM, GCM, and HFB) were compared with available experimental data for the production of the medically important radionuclides ^{67}Cu, ^{131}I, and ^{99m}Tc. The observed variations among the models are mainly attributed to differences in the treatment of nuclear level density, compound nucleus formation probability, and pre-equilibrium particle emission mechanisms implemented in EMPIRE 3.2.3.

For the ^{68}Zn(p,2p)^{67}Cu reaction shown in Figure 1, all models reproduced the general excitation-function trend with peak energies between 25 and 32 MeV, which corresponds to the energy region where compound nucleus formation and proton emission become dominant. The EGSM model produced the highest peak cross section of approximately 14 mb at 30 MeV because the model enhances the level density at moderate excitation energies through pairing and collective effects, thereby increasing the probability of compound nucleus decay through the (p,2p) channel. GSM provided the best agreement with experimental peak magnitude and energy position because its generalized treatment of shell damping and excitation-energy dependence produced more realistic transmission coefficients in this energy region. In contrast, the HFB model predicted a narrower and steeper peak around 25 MeV with lower cross-section values. This behavior may be attributed to the microscopic treatment of nuclear states in HFB, which restricts the density of accessible excited states and consequently reduces the reaction probability. The underestimation of cross sections above 40 MeV by all models suggests increasing dominance of pre-equilibrium and direct reaction mechanisms, which are more difficult to reproduce accurately using statistical compound-nucleus approaches alone.

For the ^{70}Zn(p,α)^{67}Cu reaction in Figure 2, the excitation functions peaked near 15–17 MeV, corresponding to the threshold region where alpha-particle emission becomes energetically favorable. EGSM strongly overestimated the experimental peak cross section by predicting values around 57 mb compared with the experimental value of about 15 mb. This overprediction indicates that the model may over-enhance the density of available excited states and compound-nucleus decay probability for alpha emission. GSM and GCM also produced larger peak magnitudes because of their phenomenological parameterization of level densities, which can increase particle-emission probabilities at low excitation energies. The HFB model gave the closest agreement with the experimental data in both shape and magnitude because the microscopic description of single-particle states and shell effects provides a more realistic representation of alpha-emission probabilities. The slight energy shift of the HFB peak toward 17 MeV may result from differences in optical model transmission coefficients and threshold-energy treatment within the EMPIRE calculations.

For the ^{130}Te(d,n)^{131}I reaction shown in Figure 3, all models predicted peak energies within the range of 12–17 MeV. Experimentally, the peak occurred near 17 MeV with a cross section close to 0.10 barns. The HFB model reproduced the experimental peak magnitude more accurately because microscopic level-density calculations better account for neutron-emission channels in deuteron-induced reactions. However, the peak energy was shifted toward 12 MeV, suggesting that the pre-equilibrium contribution in the model becomes significant earlier than observed experimentally. EGSM, GSM, and GCM correctly reproduced the peak energy around 17 MeV but underestimated the peak magnitude by approximately 20–30%, indicating lower predicted compound-nucleus formation probabilities. The overestimation of cross sections above 15 MeV by GCM may be linked to its simplified constant-temperature treatment of nuclear level densities, which tends to overpredict available excitation states at higher energies.

For the ^{100}Mo(p,2n)^{99m}Tc reaction in Figure 4, all models predicted maximum cross sections around 18 MeV, which corresponds to the optimum energy region for the (p,2n) reaction channel. The HFB model produced the highest peak cross section of 994.78 mb, closely followed by EGSM with 983.28 mb. The large cross-section values in this energy region are associated with strong compound-nucleus formation and favorable neutron-emission probability. The wider excitation function predicted by HFB indicates that the microscopic level-density treatment allows a broader distribution of accessible excited states, thereby increasing neutron emission over a larger energy interval. GSM and GCM predicted slightly lower peak values because their phenomenological parameterizations provide comparatively lower state densities at higher excitation energies. The superior performance of HFB in this reaction demonstrates the importance of microscopic shell and pairing effects in accurately describing neutron-emission processes relevant to ^{99m}Tc production.

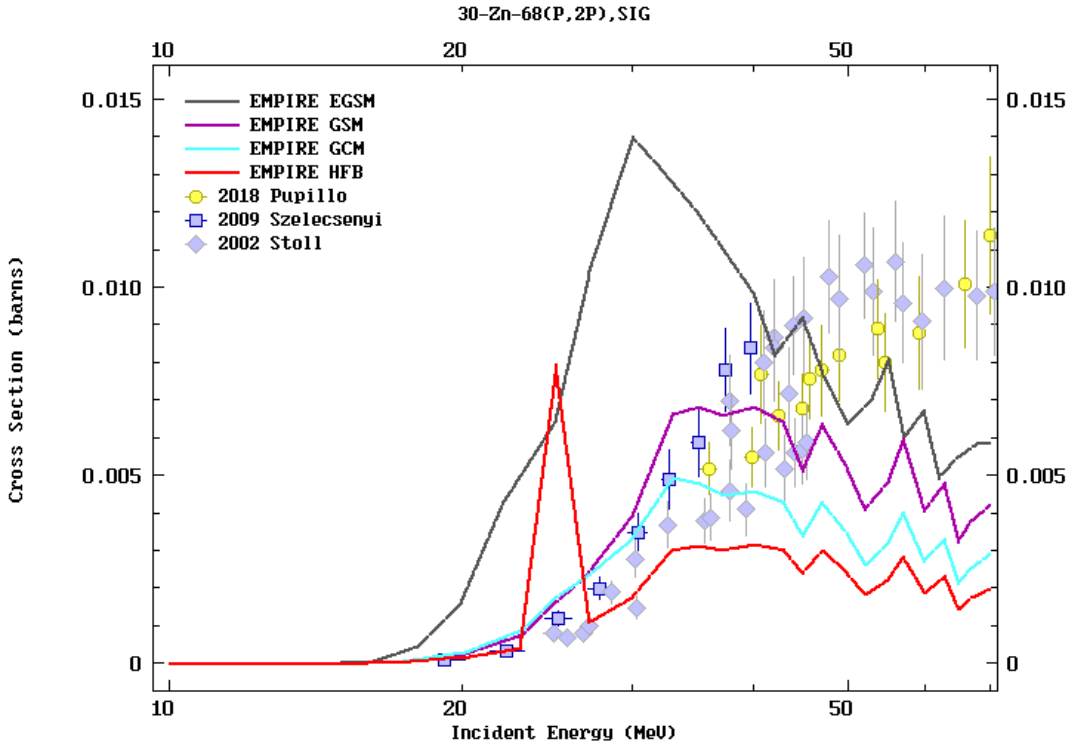


Figure 1. Calculated ^{68}Zn(p,2p) cross section from different level density models benchmarked with experimental data from EXFOR for the production of ^{67}Cu.

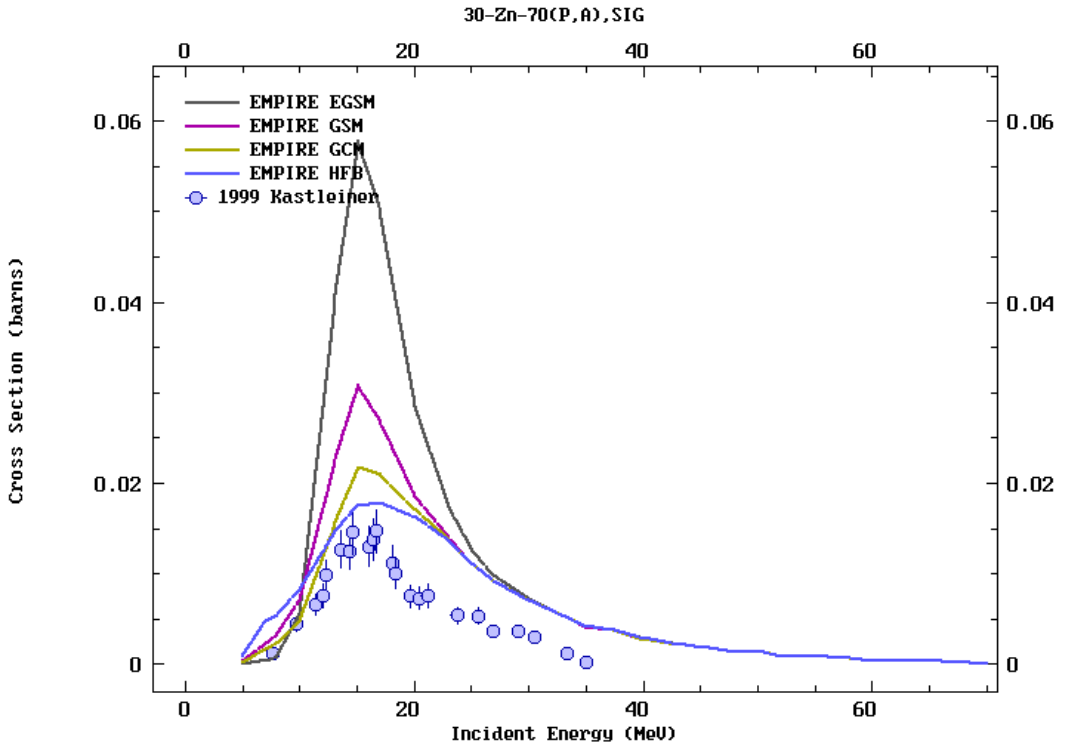


Figure 2. Calculated ^{70}Zn(p,α) cross section from different level density models benchmarked with experimental data from EXFOR for the production of ^{67}Cu.

Similarly, for the ^{100}Mo(n,2n)^{99}Mo reaction shown in Figure 5, all models exhibited a rapid rise in cross section beginning around 8 MeV, followed by peak values near 15 MeV. This behavior corresponds to the threshold for neutron multiplication reactions and the increasing probability of compound nucleus excitation. Experimental data agreed reasonably well with the theoretical curves near the peak region, confirming the predictive capability of EMPIRE for neutron-induced reactions. EGSM and GSM predicted slightly

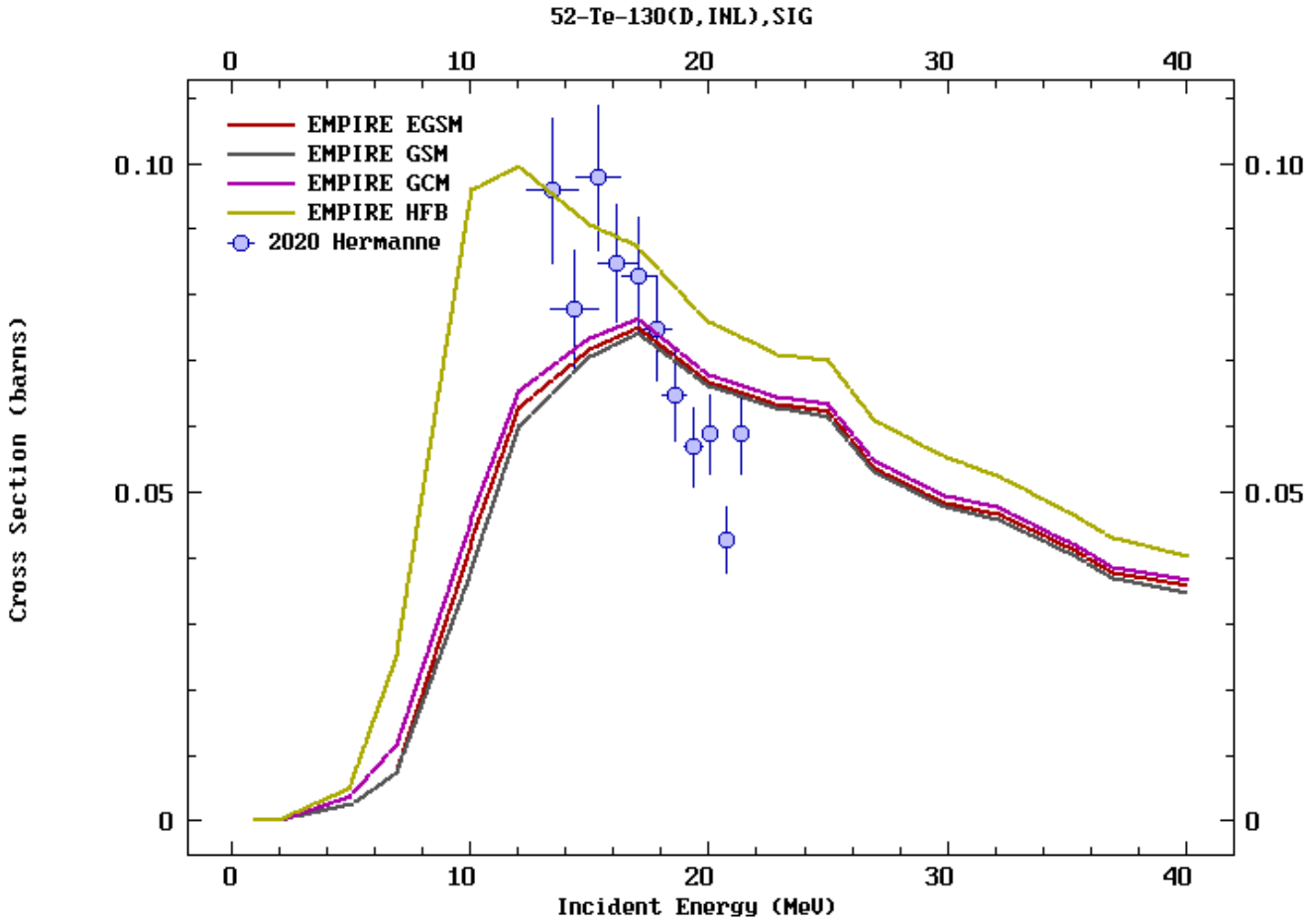


Figure 3. Calculated ^{130}Te(d,n) cross section from different level density models benchmarked with experimental data from EXFOR for the production of ^{131}I.

higher peak cross sections because their level-density formulations increase the probability of neutron emission at intermediate excitation energies. GSM gave the best overall agreement with the experimental data because its treatment of shell damping and collective enhancement provided a balanced description of both low- and high-energy reaction regions. The gradual decrease in cross section beyond 15 MeV is associated with increased competition from other reaction channels and pre-equilibrium neutron-emission processes.

Table 1 summarizes the best-performing EMPIRE level density model for the investigated reaction channels based on the benchmark results.

Table 1 presents the comparative performance of the four EMPIRE NLD models (EGSM, GSM, GCM, and HFB) for all investigated reaction channels. The evaluation was based on agreement with experimental excitation functions in terms of peak cross section, peak energy position, excitation-function shape, and overall trend across the investigated energy range.

The GSM model showed the best agreement for the ^{68}Zn(p,2p)^{67}Cu and ^{100}Mo(n,2n)^{99}Mo reactions because its treatment of shell damping and excitation-energy dependence produced more stable predictions over the relevant energy ranges. In contrast, the HFB model performed best for the ^{70}Zn(p,α)^{67}Cu, ^{130}Te(d,n)^{131}I, and ^{100}Mo(p,2n)^{99m}Tc reactions due to its microscopic description of nuclear structure effects, which improved the prediction of neutron and alpha-particle emission probabilities.

The EGSM model generally produced higher peak cross sections because of the inclusion of collective enhancement effects that increase nuclear level densities at moderate excitation energies. However, this often resulted in overestimation of experimental values, particularly in charged-particle-induced reactions. The GCM model reproduced some excitation-function trends reasonably well but showed larger deviations at higher energies due to limitations associated with its simplified phenomenological treatment of NLD.

Overall, the results indicate that the predictive capability of EMPIRE 3.2.3 strongly depends on the choice of level density model and reaction mechanism. Therefore, careful selection and validation of nuclear model parameters are necessary for reliable medical radioisotope production calculations.

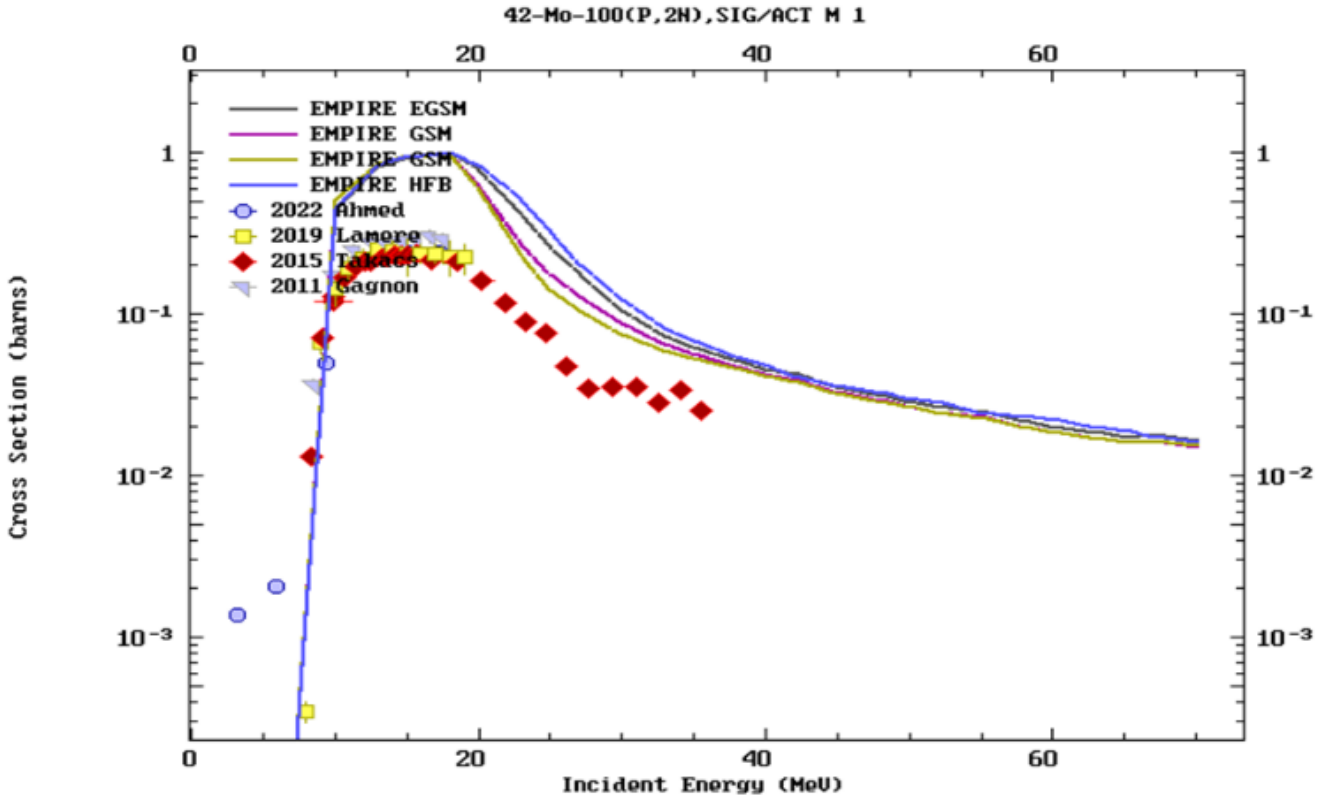


Figure 4. Calculated ^{100}Mo(p,2n) cross section from different level density models benchmarked with experimental data from EXFOR for the production of ^{99m}Tc.

Table 1. Comparative performance of EMPIRE level density models for different reaction channels.

Reaction cross section	EGSM performance	GSM performance	GCM performance	HFB performance	Best-fit model
^{68}Zn(p,2p)^{67}Cu	Overestimated peak cross section at ~30 MeV; moderate agreement at mid energies	Best agreement in peak magnitude and energy position	Moderate agreement but wider deviation above 35 MeV	Narrow peak with underestimated cross section	GSM
^{70}Zn(p,α)^{67}Cu	Strong overestimation of peak cross section	Overpredicted peak values with large fluctuations	Overestimated peak magnitude and energy spread	Best agreement in both peak shape and magnitude	HFB
^{130}Te(d,n)^{131}I	Correct peak energy but underestimated magnitude	Good peak-energy prediction with lower cross section	Overestimated cross sections above 15 MeV	Best overall agreement with experimental trend	HFB
^{100}Mo(p,2n)^{99m}Tc	Very high peak cross section close to experiment	Slightly underestimated peak values	Lower peak magnitude compared with experiment	Best prediction of yield and excitation-function width	HFB
^{100}Mo(n,2n)^{99}Mo	Slightly overestimated peak cross section	Best overall agreement with experimental data	Lower peak magnitude and broader deviation	Moderate agreement at the peak region	GSM

3.1. Purity analysis

Radionuclidic purity of the investigated medical radioisotopes were evaluated using the calculated excitation functions obtained from EMPIRE 3.2.3. The analysis was based on the best-fit cross-section (σ_p), total cross section (σ_T), purity index (PI), and optimum incident energy interval for each reaction channel.

The best-fit cross-section (σ_p) corresponds to the maximum value of the excitation function obtained from the EMPIRE calculations within the investigated energy range. The total cross section (σ_T) was obtained by summing the calculated excitation-function values over the selected optimum energy interval for each reaction channel. Thus, σ_T represents the cumulative reaction probability within the practical irradiation energy range relevant for isotope production.

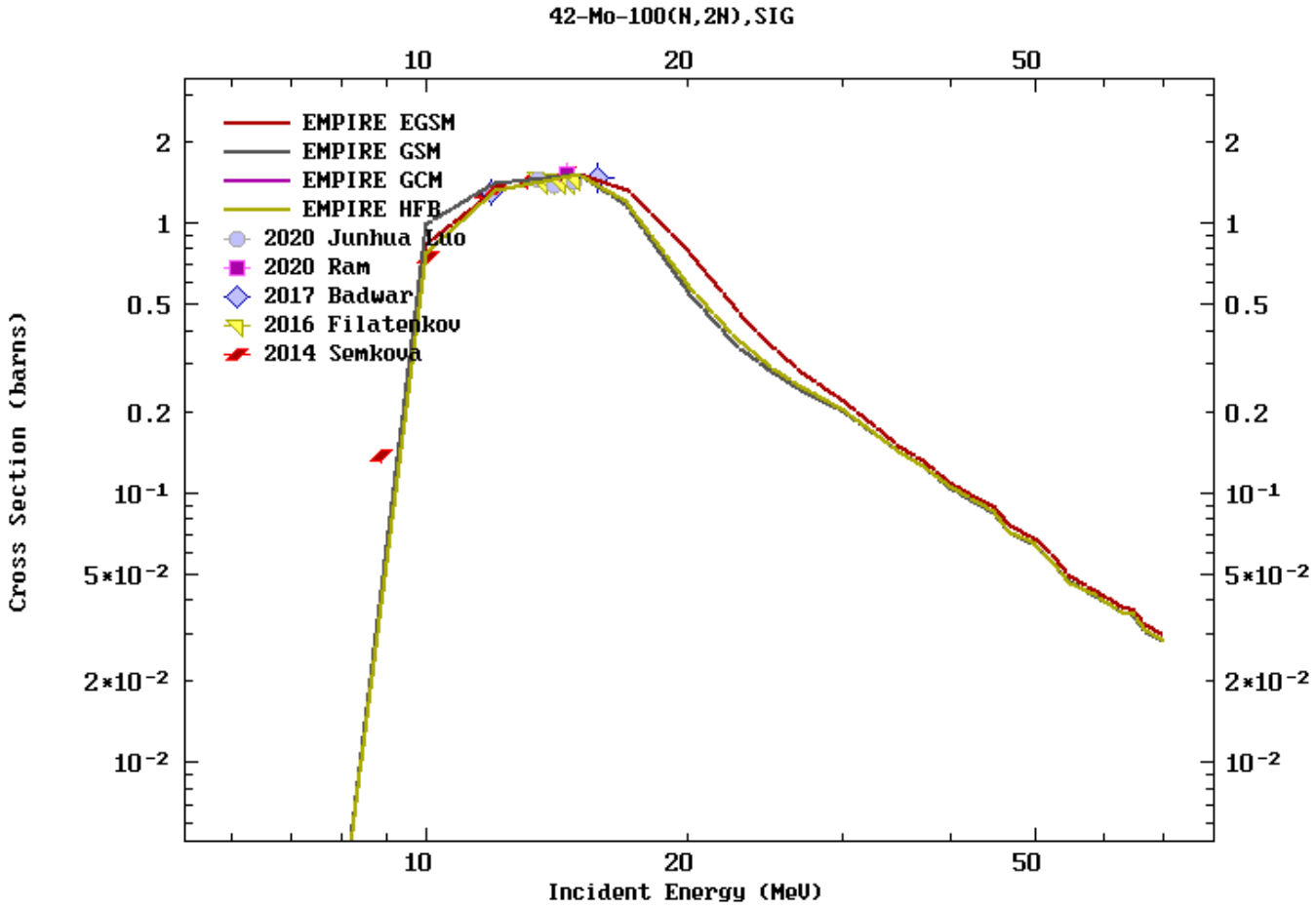


Figure 5. Calculated ^{100}Mo(n,2n) cross section from different level density models benchmarked with experimental data from EXFOR for the production of ^{99}Mo.

Table 2. Cross-section and purity parameters for selected medical radioisotope production reactions.

Radioisotope	Production reaction	Best-fit energy, E_p (MeV)	Best-fit cross-section, σ_p (mb)	Total cross section, σ_T (mb)	PI (%)	Optimum energy interval (MeV)
^{67}Cu	^{68}Zn(p,2p)^{67}Cu	32.00	6.80	158.59	4.28	30–40
^{67}Cu	^{70}Zn(p,α)^{67}Cu	17.00	17.79	154.26	11.54	10–25
^{131}I	^{130}Te(d,n)^{131}I	12.00	99.94	919.84	10.86	8–14
^{99m}Tc	^{100}Mo(p,2n)^{99m}Tc	18.00	994.78	5760.58	17.27	10–20
^{99}Mo	^{100}Mo(n,2n)^{99}Mo	15.00	1500	7819.50	19.18	10–20

The radionuclidic purity was estimated using the PI, given by [14]

$$PI = \frac{\sigma_p}{\sigma_T} \times 100\%. \tag{2}$$

A higher PI value indicates that the desired reaction channel contributes more dominantly within the irradiation energy interval and therefore results in improved radionuclidic purity with reduced contamination from competing reactions.

Table 2 summarizes the best-fit cross-sections, total cross-sections, purity indices, and optimum energy intervals for the investigated production reactions. The results reveal significant differences in the production characteristics of the selected radionuclides. Among the investigated reactions, the 100Mo(n,2n)99Mo ^{100}Mo(n,2n)^{99}Mo reaction exhibited the highest best-fit cross-section (1500.00 mb), the largest total cross-section (7819.50 mb), and the highest purity index (19.18%) within the optimum energy interval of 10–20 MeV. These results indicate that this reaction possesses the most favourable production characteristics among the investigated reaction channels under the conditions considered in this study. ^{100}Mo(p,2n)^{99m}Tc reaction also demonstrated excellent production characteristics, with a high best-fit cross-section (994.78 mb), a substantial total cross-section (5760.58 mb), and a purity index of 17.27%, confirming its suitability for the production of Technetium-99m. The ^{70}Zn(p,α)^{67}Cu reaction exhibited better production characteristics than the ^{68}Zn(p,2p)^{67}Cu route, as reflected by its higher best-fit cross-section and purity index. Similarly, the ^{130}Te(d,n)^{131}I reaction showed satisfactory agreement with experimental observations and favourable production characteristics within its optimum energy interval.

Overall, the comparative analysis demonstrates that the production characteristics of the investigated radionuclides depend on the combined influence of the best-fit cross-section, integrated reaction probability, purity index, and optimum irradiation energy rather than on any single parameter alone.

4. Conclusion

In this analysis, the nuclear reaction model code EMPIRE 3.2.3 was used to assess the production cross-sections of major medical radionuclides through the reactions ^{68}Zn(p,2p)^{67}Cu, ^{70}Zn(p,α)^{67}Cu, ^{130}Te(d,n)^{131}I, ^{100}Mo(p,2n)^{99m}Tc, and ^{100}Mo(n,2n)^{99}Mo. The evaluations were calculated from threshold energy to 70 MeV with optimized nuclear level density parameters used to simulate and compare with experimental data. The findings provide evidence of the high sensitivity of reaction cross-sections to the selected nuclear level density model. Based on comparison with experimental data and benchmarking with evaluated nuclear data libraries from the IAEA, the most appropriate models for each reaction channel were determined in Table 1.

Comparative analysis of the best-fit cross-sections, total cross-sections, and purity indices indicated that the production characteristics of the investigated reactions are ranked as follows: $^{100}\mathrm{Mo}(n,2n)^{99}\mathrm{Mo} >^{100} \mathrm{Mo}(p,2n)^{99m}\mathrm{Tc} >^{130} \mathrm{Te}(d,n)^{131}\mathrm{I} >^{70} \mathrm{Zn}(p,\alpha)^{67}\mathrm{Cu} >^{68} \mathrm{Zn}(p,2p)^{67}\mathrm{Cu}$. Similarly, the radionuclidic purity followed the order: $^{100}\mathrm{Mo}(n,2n)^{99}\mathrm{Mo} >^{100} \mathrm{Mo}(p,2n)^{99m}\mathrm{Tc} >^{70} \mathrm{Zn}(p,\alpha)^{67}\mathrm{Cu} >^{130} \mathrm{Te}(d,n)^{131}\mathrm{I} >^{68} \mathrm{Zn}(p,2p)^{67}\mathrm{Cu}$. These findings suggest that the $^{100}\mathrm{Mo}(n,2n)^{99}\mathrm{Mo}$ reaction exhibits the most favourable production characteristics among the investigated reactions, based on its highest best-fit cross-section, total cross-section, and purity index. The $^{100}\mathrm{Mo}(p,2n)^{99m}\mathrm{Tc}$ reaction also demonstrated excellent production characteristics and remains an attractive route for the production of Technetium-99m under suitable irradiation conditions. Conversely, the $^{68}\mathrm{Zn}(p,2p)^{67}\mathrm{Cu}$ reaction exhibited comparatively lower best-fit cross-sections and purity, indicating less favourable production characteristics than the alternative $^{70}\mathrm{Zn}(p,\alpha)^{67}\mathrm{Cu}$ route.

Data availability

Data will be made available upon reasonable request from the corresponding author.

Declaration of competing interest

The authors declare that they have no known competing financial interests or personal relationships that could have appeared to influence the work reported in this manuscript.

Funding

The authors received no external funding for this study.

References

[1] S. C. Vaz, F. Oliveira, K. Herrmann & P. Veit-Haibach, “Nuclear medicine and molecular imaging advances in the 21st century”, British Journal of Radiology **93** (2020) 20200095. https://doi.org/10.1259/bjr.20200095.

[2] S. M. Qaim, “Nuclear data relevant to the production and application of diagnostic radionuclide”, Radiochimica Acta **89** (2001) 223. https://doi.org/10.1524/ract.2001.89.4-5.223.

[3] W. D. Loveland, D. J. Morrissey & G. T. Seaborg, *Modern nuclear chemistry*, Wiley-Interscience, Hoboken, NJ, USA, 2006. https://doi.org/10.1002/0471768626.

[4] T. T. Böhlen, F. Cerutti, M. P. W. Chin, A. Fassò, A. Ferrari, P. G. Ortega, A. Mairani, P. R. Sala, G. Smirnov & V. Vlachoudis, “The FLUKA code: developments and challenges for high energy and medical applications”, Nuclear Data Sheets **120** (2014) 211. https://doi.org/10.1016/j.nds.2014.07.049.

[5] A. B. Olorunsola, J. A. Bamikole, A. A. Bello & O. O. Ige, “Theoretical prediction of neutron-induced radiative capture cross section of some isotopes of minor actinides”, Journal of Nuclear and Radiation Sciences **2** (2023) 1. http://dx.doi.org/10.5455/jnrs.2023.01.001.

[6] D. A. Brown, M. B. Chadwick, R. Capote, A. C. Kahler, A. Trkov, M. W. Herman, A. A. Sonzogni, Y. Danon, A. D. Carlson, M. Dunn, D. L. Smith, G. M. Hale, G. Arbanas, R. Arcilla, C. R. Bates, B. Beck, B. Becker, F. Brown, R. J. Casperson, J. Conlin, D. E. Cullen, M.-A. Descalle, R. Firestone, T. Gaines, K. H. Guber, A. I. Hawari, J. Holmes, T. D. Johnson, T. Kawano, B. C. Kiedrowski, A. J. Koning, S. Kopecky, L. Leal, J. P. Lestone, C. Lubitz, J. I. Márquez Damián, C. M. Mattoon, E. A. McCutchan, S. Mughabghab, P. Navratil, D. Neudecker, G. P. A. Nobre, G. Noguere, M. Paris, M. T. Pigni, A. J. Plompen, B. Pritychenko, V. G. Pronyaev, D. Roubtsov, D. Rochman, P. Romano, P. Schillebeeckx, S. Simakov, M. Sin, I. Sirakov, B. Sleaford, V. Sobes, E. S. Soukhovitskii, I. Stetcu, P. Talou, I. Thompson, S. van der Marck, L. Welser-Sherrill, D. Wiarda, M. White, J. L. Wormald, R. Q. Wright, M. Zerkle, G. Žerovnik & Y. Zhu, “ENDF/B-VIII.0: The 8th major release of the nuclear reaction data library with CIELO-project cross sections, new standards and thermal scattering data”, Nuclear Data Sheets **148** (2018) 1. https://doi.org/10.1016/j.nds.2018.02.001.

[7] A. Koning, S. Hilaire & S. Goriely, “TALYS: Modeling of nuclear reactions,” The European Physical Journal A **59** (2023) 131. https://doi.org/10.1140/epja/s10050-023-01034-3.

[8] A. J. Koning & D. Rochman, “Modern nuclear data evaluation with the TALYS code system”, Nuclear Data Sheets **113** (2012) 2841. https://doi.org/10.1016/j.nds.2012.11.002.

[9] W. Hauser & H. Feshbach, “The inelastic scattering of neutrons”, Physical Review **87** (1952) 366. https://doi.org/10.1103/PhysRev.87.366.

[10] A. Gilbert & A. G. W. Cameron, "A composite nuclear-level density formula with shell corrections," Canadian Journal of Physics **43** (1965) 1446. https://doi.org/10.1139/p65-139.
[11] A. V. Ignatyuk, G. N. Smirenkin & A. S. Tishin, "Phenomenological description of the energy dependence of the level density parameter," Soviet Journal of Nuclear Physics **21** (1975) 255. https://doi.org/10.1007/BF01125206.
[12] S. Goriely, S. Hilaire & A. J. Koning, "Improved microscopic nuclear level densities within the Hartree–Fock–Bogoliubov plus combinatorial method", Physical Review C **78** (2008) 064307. https://doi.org/10.1103/PhysRevC.78.064307.
[13] H. A. Bethe, "Nuclear Physics B. Nuclear Dynamics, Theoretical," Reviews of Modern Physics **9** (1937) 69. https://doi.org/10.1103/RevModPhys.9.69.
[14] S. Takács, Z. Szűcs, F. Tárkányi, A. Hermanne & M. Sonck, "Evaluation of proton-induced reactions on ^{100}Mo: new cross sections for production of ^{99m}Tc and ^{99}Mo", Journal of Radioanalytical and Nuclear Chemistry **257** (2003) 195. https://doi.org/10.1023/A:1024790520036.